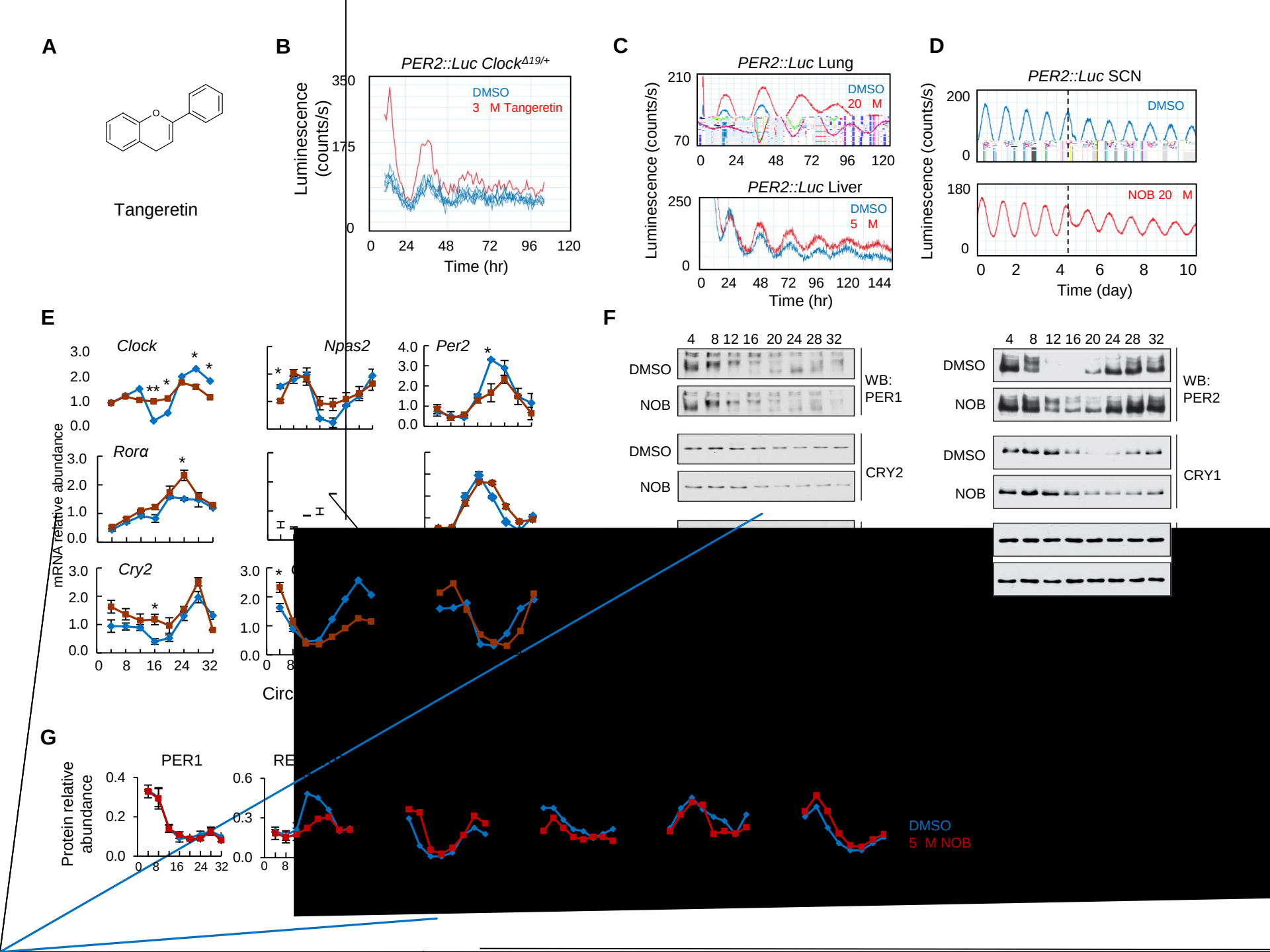
A
Tangeretin
B
PER2::Luc Clock Δ19/+
Luminescence (counts/s)
DMSO
3 M Tangeretin
Time (hr)
C
PER2::Luc Lung
DMSO
20 M
PER2::Luc Liver
DMSO
5 M
Luminescence (counts/s)
Time (hr)
D
PER2::Luc SCN
DMSO
NOB 20 M
Luminescence (counts/s)
Time (day)
E
Clock
Npas2
Per2
Rorα
Cry2
mRNA relative abundance
F
DMSO
NOB
WB: PER1
CRY2
WB: PER2
CRY1
G
PER1
Protein relative abundance
DMSO
5 M NOB

Figure S1. Effects of NOB and Tangeretin on circadian reporter rhythms and clock gene expression in cells and tissue explants. Related to Figure 1.

(A) Structures of Tangeretin.

(B) Identification of Tangeretin as a clock-enhancing molecule. Fully confluent *PER2::LUC Clock*$^{\Delta 19/+}$ reporter cells were first stimulated with Fsk for 1 hr and compounds were added to the plate. Reporter luminescence was recorded over 4 days in an EnVision microplate reader.

(C) Clock-enhancing effects of NOB in peripheral tissues including lung (top) and liver (C, bottom) explant from *PER2::Luc* WT reporter mice. The graphs are representative of at least three experiments.

(D) NOB did not enhance reporter rhythms in SCN explants from *PER2::Luc* WT reporter mice. Media were changed after 7 days of culture (day 0). DMSO or NOB was administered at the indicated times (Dashed line). No amplitude enhancement by NOB was observed comparing rhythms before and after NOB administration.

(E) mRNA level expression of clock genes analyzed by real-time qPCR in *PER2::LucSV* cells pretreated with Fsk for 1 hr.

(F) Representative Western blots of circadian clock proteins in cells as treated in (E).

(G) Quantification of Western blot (n=2-3) analysis for clock proteins in (F).

Data are represented as mean ± SEM. **p* < 0.05, ***p* < 0.01 and ****p* < 0.001. NOB vs. DMSO.

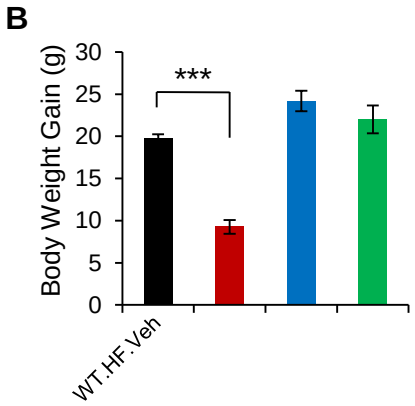
B
Body Weight Gain (g)
30
25
20
15
10
5
0
***
WT.HF.Veh

Figure S2. Pharmacokinetics of NOB and distinct effects of NOB on high fat diet-fed wild-type (WT) and *Clock*$^{\Delta 19/\Delta 19}$ mutant mice. Related to Figures 2 and 3.

(A) NOB levels in mouse plasma, brain and liver were determined by LC-MS/MS by following administration by oral gavage at a dose of 200mg/kg of body weight (n=3).

(B J) WT or *Clock*$^{\Delta 19/\Delta 19}$ mutant mice were fed high-fat (HF) diet and treated with either vehicle or NOB every other day (n=8-15).

(B) Body weight gains at the end of the 10-week treatment period are shown (n=8-15).

(C) Food intake amount during dark (solid) and light (open) phases corresponding to subjective night and day. The Y axis indicates cumulative food intake for the dark or light phase (n=8-15).

(D) NOB reduced visceral WAT cell size. Image from three sections 200 m apart were analyzed, representing >500 cells.

(E) VO_2 (volume of oxygen consumed) for each group was quantified for dark (solid bars) and light (open bars) phases (n=8).

(F) Energy expenditure was recorded over the circadian cycle (n=8).

(G) Respiratory quotient was quantified for dark and light phases (n=8).

(H, I) Weight (H) and representative images (I) of whole livers from HFD-fed WT and *Clock*$^{\Delta 19/\Delta 19}$ mutant mice treated with Vehicle or NOB (n=8-15).

(J) Histological analysis of liver after 10-week treatment. Liver were stained with oil red O to visualize lipid droplets.

Data are represented as mean ± SEM. One-way ANOVA was performed using the SigmaStat software. *$p < 0.05$, *** $p < 0.01$ and ***$p < 0.001$. WT.HF.NOB vs. WT.HF.Veh. $^{###}p < 0.001$. Clk.HF.Veh vs. WT.HF.Veh.

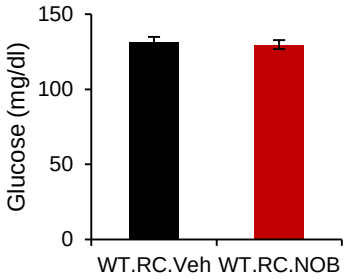
150
100
50
0
Glucose (mg/dl)
WT.RC.Veh
WT.RC.NOB

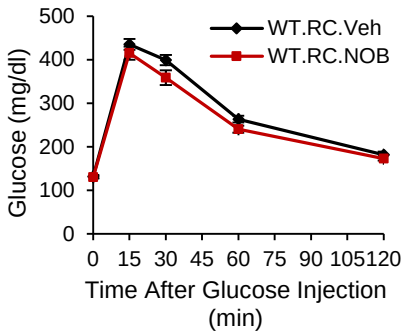
500
400
300
200
100
0
Glucose (mg/dl)
WT.RC.Veh
WT.RC.NOB
0 15 30 45 60 75 90 105120
Time After Glucose Injection
(min)

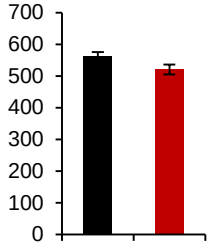
700
600
500
400
300
200
100
0

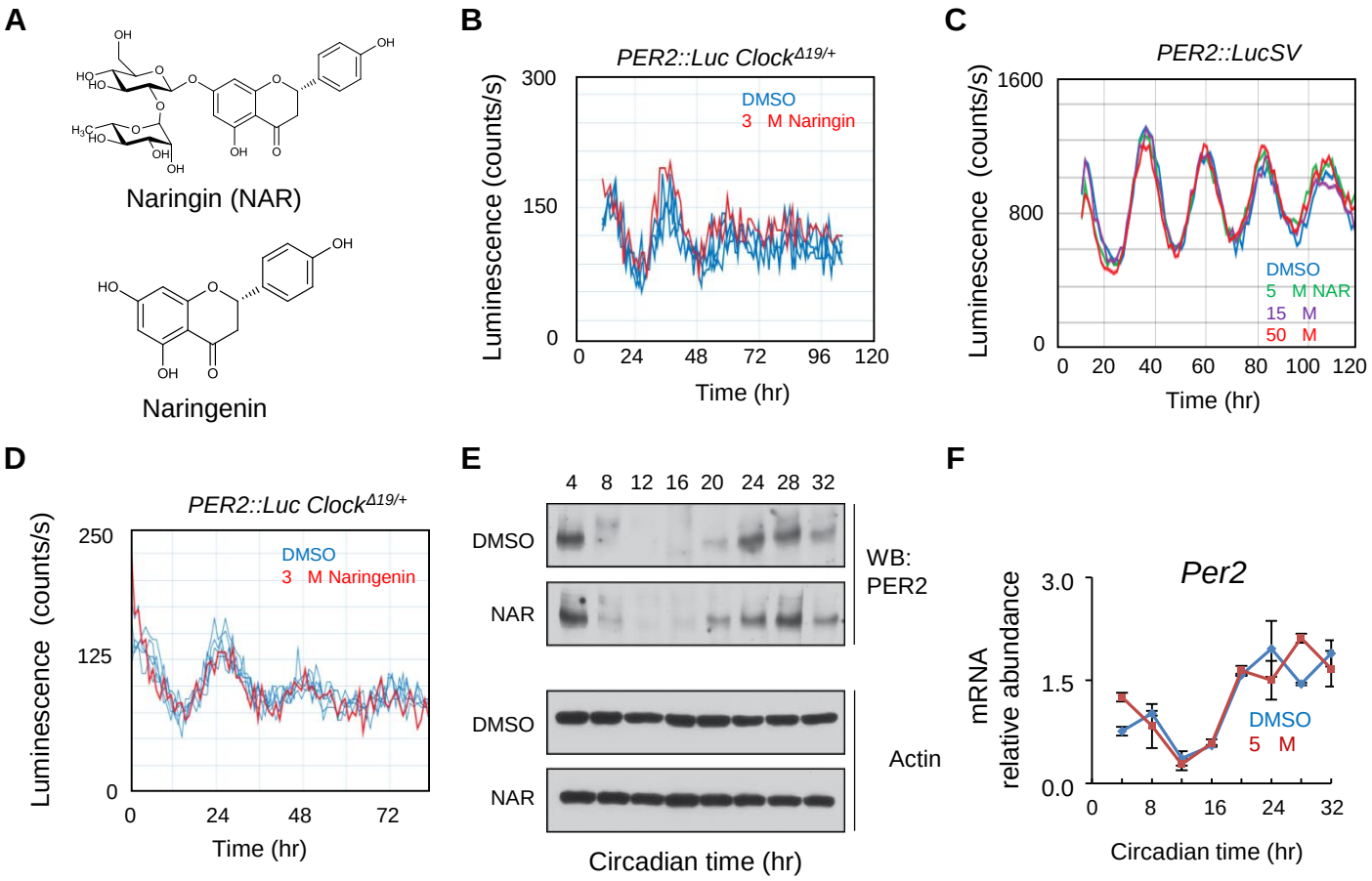

Figure S4. Naringin and Naringenin are clock-inactive analogs. Related to Figures 2 and 3.
(A) Structures of Naringin (NAR) and Naringenin.
(B-D) Naringin (B, C) and Naringenin (D) did not enhance the reporter luminescence in *PER2::LucSV* or *PER2::LUC Clock*$^{\Delta 19/+}$ reporter cells.
(E) Western blot analysis of PER2 protein in *PER2::LucSV* cells. Cells were treated with 5 μM of NAR or DMSO at time 0, and collected every 4 hrs up to 32 hrs followed by immunoblotting with antibody.
(F) Real-time qPCR analysis of *Per2* mRNA level in the above treated *PER2::LucSV* cells.

A

B

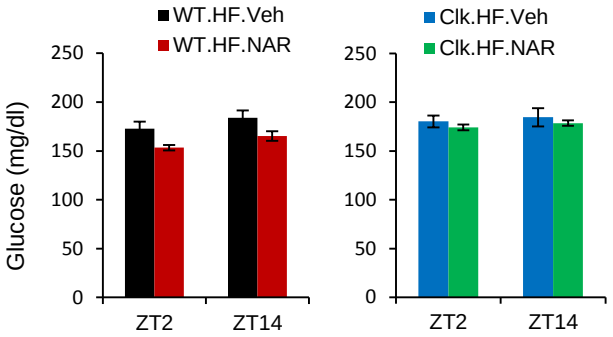
WT.HF.Veh
WT.HF.NAR
Clk.HF.Veh
Clk.HF.NAR
Glucose (mg/dl)
250
200
150
100
50
0
ZT2
ZT14

C

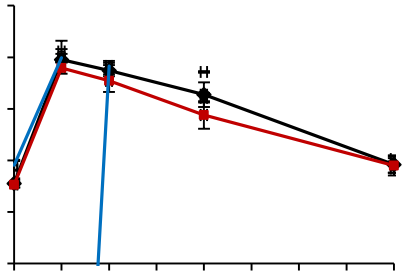

D

E

F

G

Figure S5. Effects of Naringin (NAR) on body weight, glucose and lipid homeostasis in HFD-fed WT and *Clock*$^{\Delta 19/\Delta 19}$ mutant mice. Related to Figures 2 and 3.

(A) Average body weight (left panel) and body weight gain (right panel) for HFD-fed mice treated with vehicle or NAR (WT.HF.Veh, WT.HF.NAR, Clk.HF.Veh and Clk.HF.NAR) after 10-week treatment (n=8-15).

(B) NAR reduced fasting blood glucose levels in WT mice but not *Clock*$^{\Delta 19/\Delta 19}$ mutant mice at daytime and nighttime (n=8-15).

(C) NAR showed modest effects on glucose tolerance that were indistinguishable between WT and *Clock*$^{\Delta 19/\Delta 19}$ mutant mice as measured by glucose tolerance test (GTT) (n=8-15). Quantification of the area under curve (AUC) is also shown.

(D) NAR showed modest effects on insulin sensitivity that were indistinguishable between WT and *Clock*$^{\Delta 19/\Delta 19}$ mutant mice as measured by insulin tolerance test (ITT) (n=8-15). Quantification of the area under curve (AUC) from ITT is also shown.

(E) Blood insulin levels was decreased to similar extents by NAR in WT and *Clock*$^{\Delta 19/\Delta 19}$ mutant mice (n=8-15).

(F and G) Blood total triglyceride (TG) (F) levels and cholesterol (TC) (G) levels after 10-week treatment (n=8-15).

Data are presented as mean ± SEM. One-way ANOVA was performed by using the SigmaStat software. *$p < 0.05$. WT.HF.NAR vs. WT.HF.Veh.

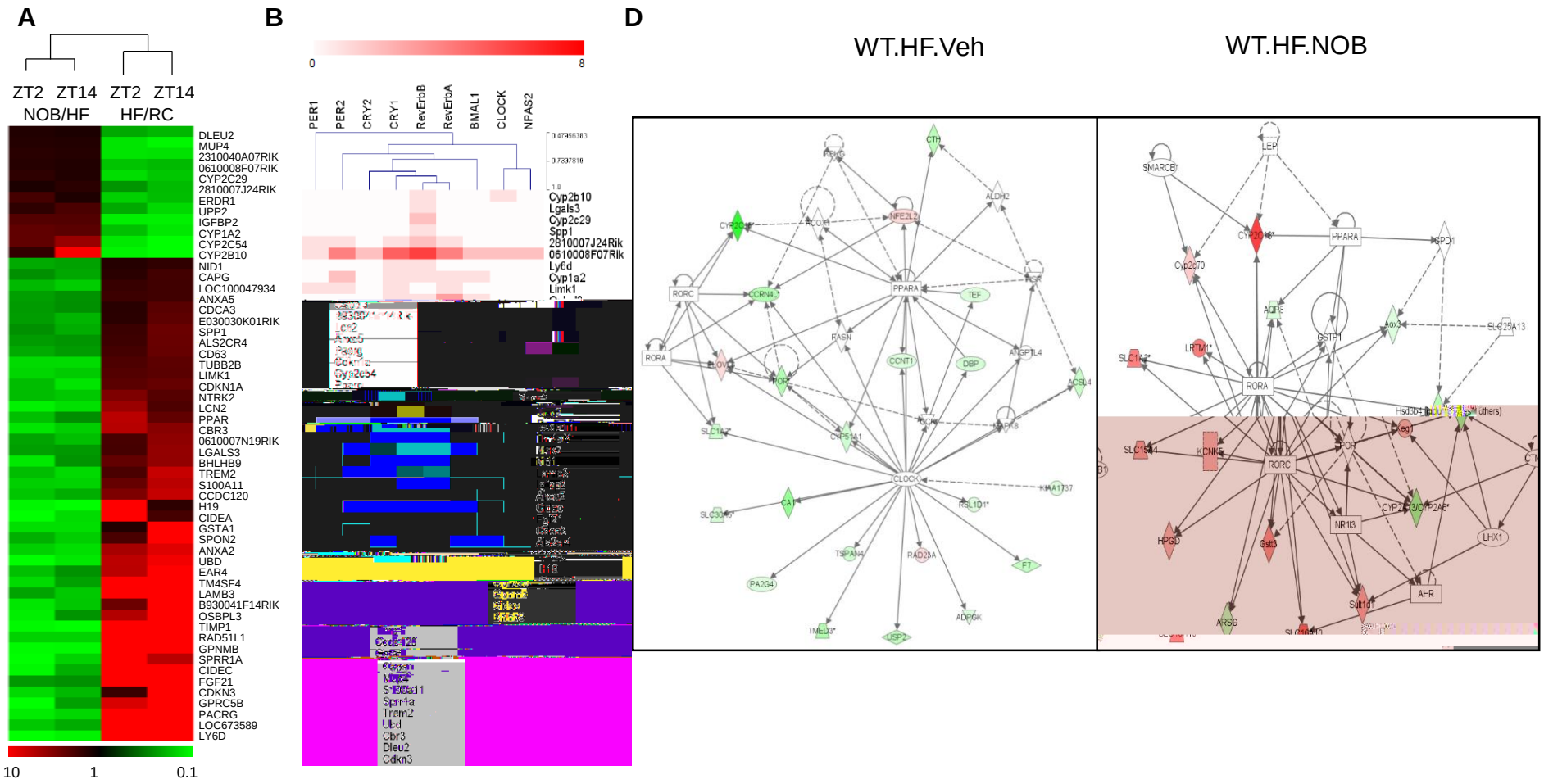

Figure S6. Clock protein binding on NOB-responsive genes and genetic/genomic analysis of ROR function in NOB response. Related to Figures 5 and 6.

(A) Ratio heat map. The expression data in Fig. 5C were computed to derive fold change indicating that the expression patterns of 56 genes altered by HFD were reversed by NOB in mouse liver at both ZT2 and ZT14 time points. Color scale shows fold change (ratio). NOB/HF indicates HF.NOB vs. HF.Veh expression ratio; HF/RC indicates HF.Veh vs. RC.Veh expression ratio. (B) Thirty one genes show clock protein binding, whereas the remaining genes do not (blank area). Analysis was based on published ChIP-Seq results (Koike et al., 2012; Cho et al. 2012). The red scale indicates magnitude of DNA occupancy as quantified by enrichment of immunoprecipitated DNA fragments bound for each transcription factor. (C) (Left) and (Right) mRNA expression in Hepa1-6 cells treated with control (Ctrl) or mouse siRNA, and vehicle (DMSO) or NOB (3 , 12 h) (n=4). (D) Highlighted within the network is ROR / that functions as a nodal point for genes regulated by NOB. Genes down- and up-regulated by HFD (left) or NOB (right) are indicated by green and pink respectively, with the color intensity corresponding to fold changes.

changes by NOB at both ZT2 and ZT14. This gene set was annotated from a total of 56 genes.

Category	Gene Product	Description
Lipid metabolism	ANXA5	Annexin A5
	OSBPL3	Oxysterol-binding protein-related protein 3
	CYP2C54	Cytochrome P450 2C54
	CYP2B10	Cytochrome P450 2B10
	ANXA2	Annexin A2
	LCN2	Neutrophil gelatinase-associated lipocalin
	CBR3	Carbonyl reductase [NADPH] 3
Protein metabolism	MUP4	Major urinary protein 4
	PPARG	Peroxisome proliferator-activated receptor gamma
	CYP2C29	Cytochrome P450 2C29
	2810007J24RIK	Protein 2810007J24Rik
	CYP1A2	Cytochrome P450 1A2
DNA metabolism	CDKN3	Cyclin-dependent kinase inhibitor 3
	TIMP1	Metalloproteinase inhibitor 1
	UBD	Ubiquitin D
	LAMB3	Laminin subunit beta-3
	NTRK2	BDNF/NT-3 growth factors receptor
	LIMK1	LIM domain kinase 1
	RAD51L1	RAD51 homolog B (S. cerevisiae)
	S100A11	S100 calcium binding protein A11
Signal transduction	S100A11	S100 calcium binding protein A11
	ANXA5	Annexin A5
	IGFBP2	Insulin-like growth factor-binding protein 2
	NID1	Nidogen-1
	CD63	CD63 antigen
	ANXA2	Annexin A2
	LCN2	Neutrophil gelatinase-associated lipocalin
	GPRC5B	G-protein coupled receptor family C group 5 member B
	LAMB3	Laminin subunit beta-3
Electron transport chain	NTRK2	Cytochrome P450 2C29
	CYP1A2	Cytochrome P450 1A2
RNAP II transcription	PPARG	Peroxisome proliferator-activated receptor gamma
	ANXA5	Annexin A5
	OSBPL3	Oxysterol-binding protein-related protein 3
	TUBB2B	Tubulin beta-2B chain
Transport	ANXA2	Annexin A2
	LCN2	Neutrophil gelatinase-associated lipocalin
	LAMB3	Laminin subunit beta-3
	MUP4	Major urinary protein 4

Table S2, related to Figures 5 and 6. Sequences of qPCR primers used.

Gene Name	Forward Primer	Reverse Primer
mAdipq	TGTTCCTCTTAATCCTGCCCA	CCAACCTGCACAAGTTCCCTT
mApoa1	GGCACGTATGGCAGCAAGAT	CCAAGGAGGAGGATTCAAACTG
mApoa4	CCAATGTGGTGTGGGATTACTT	AGTGACATCCGTCTTCTGAAAC
mApoc2	ACCTGTACCAGAAGACATACCC	CCTGCGTAAGTGCTCATGG
mBmal1	CCAAGAAAGTATGGACACAGACAA A	GCATTCTTGATCCTTCCTTGG T
mCD36	CAAGCTCCTTGGCATGGTAGA	TGGATTTGCAAGCACAATATGAA
mCidec	ATGGACTACGCCATGAAGTCT	CGGTGCTAACACGACAGGG
mClock	CCTTCAGCAGTCAGTCCATAA AC	AGACATCGCTGGCTGTGTTAA
mCry1	CTGGCGTGGAAGTCATCG T	CTGTCCGCCATTGAGTTCTAT G
mCry2	TGTCCCTTCCTGTGTGGAAGA	GCTCCCAGCTTGGCTTGA
mCyp7a1	GGGATTGCTGTGGTAGTGAGC	GGTATGGAATCAACCCGTTGTC
mCyp7b1	GGAGCCACGACCCTAGATG	TGCCAAGATAAGGAAGCCAAC
mDbp	CGTGGAGGTGCTTAATGACCTTT	CATGGCCTGGAATGCTTGA
mGAPDH	CAAGGTCATCCATGACAACTTTG	GGCCATCCACAGTCTTCTGG
mGCK	TGAGCCGGATGCAGAAGGA	GCAACATCTTTACACTGGCCT
mGlut2	TCAGAAGACAAGATCACCGGA	GCTGGTGTGACTGTAAGTGGG
mIgfbp2	CAGACGCTACGCTGCTATCC	CCCTCAGAGTGGTCGTCATCA
mIkBa	GCACTTGGCAATCATCCACG	GTATTTCCTCGAAAGTCTCGGAG
mPdk4	CCGCTGTCCATGAAGCA	GCAGAAAAGCAAAGGACGTT
mPer1	CCCAGCTTTACCTGCAGAAG	ATGGTCGAAAGGAAGCCTCT
mPer2	TGTGCGATGATGATTCGTGA	GGTGAAGGTACGTTTGGTTTGC
mPGC-1 r	TATGGAGTGACATAGAGTGTGCT	CCACTTCAATCCACCCAGAAAG
mPkm2	TGGATGTTGGCAAGGCCCGA	AGGGCCATCAAGGTACAGGCACT
mPlin2	GACCTTGTGTCCTCCGCTTAT	CAACCGCAATTTGTGGCTC
P 3 3 $ 5	CAAGAATACCAAAGTGCGATCAA	GAGCTGGGTCTTTTCAGAATAATAAG
mRev-erb r	CATGGTGCTACTGTGTAAGGTGTGT	CACAGGCGTGCACTCCATAG
mRev-erb t	TGAACGCAGGAGGTGTGATTG	GAGGACTGGAAGCTATTCTCAGA
mROR r	GCACCTGACCGAAGACGAAA	GAGCGATCCGCTGACATC A
P 5 2 5	TCAGCGCCCTGTGTTTTT C	GAGAACCAGGGCCGTGTAG
mScd1	TTCTTGCGATACACTCTGGTGC	CGGGATTGAATGTTCTTGTCGT
mVldlr	GGCAGCAGGCAATGCAATG	GGGCTCGTCACTCCAGTCT

Supplemental Experimental Procedures

Animals and cell lines. Animal husbandry for all the studies except tissue explant experiments was carried out under IACUC guidelines and the procedures were conducted as described in an animal protocol approved by the University of Texas Health Science Center at Houston (UTHSC-H). Male wild-type (WT), *Clock*$^{\Delta 19/\Delta 19}$, *db/db* and *db/db Clock*$^{\Delta 19/\Delta 19}$ mice, all on the C57BL/6J genetic background, were obtained as littermates from heterozygous breeding using *Clock*$^{\Delta 19/+}$ (Antoch et al., 1997; King et al., 1997) and *db/+* breeders obtained from the Takahashi lab and the Jackson Laboratory, #000697, respectively. Mice were group-housed (2-4/cage) in a standard animal facility under a 12hr:12hr light:dark cycle. Mice showing aggressive behaviors toward cage mates were removed. For circadian locomotor and metabolic chamber studies, mice were single-housed in a satellite facility approved by the Animal Welfare Committee of UTHSC-H. *PER2::Luc* reporter knock-in mice used for tissue explant experiments were maintained according to guidelines from IACUC at the University of Texas Southwestern Medical Center (UTSW). Adult mouse ear fibroblast and mouse embryonic fibroblast (MEF) cells were previously described (Chen et al., 2012).

High-throughput chemical screen and validation. The chemical screen for circadian clock modulators was conducted at the Chemical Genomics Core facility at the UTHSC-H. The in-house chemical library we screened consists of compounds from NIH Clinical Collection, NCI collection and Microsource Spectrum Collection. Please refer to the current website for more information regarding the screening facility and library http://cprit.rice.edu/Resources/Resources/ . The screening was conducted largely based on the protocol previously described (Chen et al., 2012). Briefly, 15,000 immortalized fibroblast cells from *Clock*$^{\Delta 19/+}$ heterozygous mice expressing the *PER2::Luc* bioluminescence reporter were plated into each well of 96-well plates, and incubated for 3–4 d to allow growth to confluency. Cells were then incubated with 5 μM forskolin for 1–2 h followed by the addition of chemical compounds to the plates with robotic arms (Beckman), and then subjected to continuous monitoring over several days in a temperature-controlled EnVision microplate reader (Perkin Elmer). Data analysis was carried out by using the MultiCycle software (Actimetrics) for measurement of period, phase, and amplitude. Among the compounds that showed greater than 2X SD effects on circadian amplitude and/or period, Nobiletin (NOB) was identified independently from two sub-libraries to significantly enhance circadian amplitude. NOB and a structurally related analog Naringin (NAR) were re-ordered from commercial sources including Sigma and GenDEPOT and dose response validation was conducted using *PER2::LucSV* reporter fibroblast cells which express stronger bioluminescence signals and thus allow precise measurements of circadian clock effects of compounds (Chen et al., 2012). Tissue explant experiments were conducted as described previously (Chen et al., 2012).

Circadian locomotor activity. RC-fed WT, HFD-fed WT and *Clock*$^{\Delta 19/\Delta 19}$ mice with NOB or Vehicle treatment were used for circadian locomoter activity experiments. Briefly, mice were first maintained for at least 2 weeks in a 12hr:12hr light:dark (LD) cycle, then released into the constant darkness, free-running condition. The mice were then maintained in constant darkness for another 2 weeks. Wheel-running data was downloaded as VitalView data files and analyzed with the ActiView and Actogram J program (Schmid et al., 2011

indicated level based on several reasons. First, previous *in vivo* studies have used similar overall amounts for mouse treatment (100-125mg/kg/day) (Lee et al., 2013; Li et al., 2006). We usually conducted the oral gavage procedure in late afternoon (ZT8-10) prior to the start of their active phase, reasoning that this may coincide with the time-window adopted by previous studies. Second, we purposely chose not to conduct daily dosing to avoid entraining the experimental mice with the procedure *per se* as an artificial zeitgeber. Furthermore, we also performed pilot pharmacokinetic (PK) assays under a single-dose condition (Fig. S7). Consistent with a favorable PK profile, we observed significant exposure in serum, brain and particularly liver. Although NOB generally became undetectable 8 hr after single-dose administration in our study, other studies were able to measure NOB levels 24 hr after administration (Kumar et al., 2012; Singh et al., 2011). Therefore, we reasoned that every-other-day dosing helps avoid any incomplete daily clearance over the chronic experimental period (10 weeks).

Weekly body weight was monitored in different treatment mice for 10 weeks. Body mass composition was measured at the end of experiments using a minispec mqNMR spectrometer (Bruker Optics, Texas) (Garcia et al., 2013). A control group of mice were fed with regular chow diet (Purina 5001) in parallel with the two treatment groups in HFD. For *db/db* and *db/db Clock*$^{\Delta 19/\Delta 19}$ mice, male mice at 6-8 weeks of age were group-housed (2-3/cage) and maintained on regular chow diets. Mice were subjected to oral gavage with either DMSO or NOB as described above.

Pharmacokinetic study in mice. NOB was administered orally at ZT8 at a dose of 200 mg/kg in 0.25% sodium Carboxy Methyl Cellulose (CMC) suspension. Three mice per time point were sacrificed at 0.0, 1.0, 2.0, 4.0, 8.0 and 24.0 hr after oral gavage. NOB in plasma, brain and liver was determined by LC-MS/MS (API 4000: EQ-RS-MS-006).

Energy expenditure and food intake measurements. Energy expenditure was examined by measuring oxygen consumption with indirect calorimetry as described (Chutkow et al., 2010; Daniels et al., 2010). After 8 weeks of treatments described above, mice from each group were placed at room temperature (22°C–24°C) in the chambers of a Comprehensive Lab Animal Monitoring System (CLAMS, Columbus Instruments, Columbus, OH). After mice adapted to the metabolic chamber, volume of O_2 consumption and CO_2 production was continuously recorded over a 24-hr period. Average O_2 consumption was calculated and compared between different treatments. Food and water were provided *ad libitum*. To measure food intake, food pellets were weighted every three hours over a 24-hr period in mice treated as above. The daily food intake was calculated from averaged food intake of 3 independent experiments.

Serum and liver lipid assays. Serum samples were obtained at ZT2 from treated mice as previously described (Jeong et al., 2015). Hepatic triglyceride and cholesterol were extracted as previously described (Liu et al., 2012). The triglyceride and cholesterol levels in liver and serum were assessed by Serum Triglyceride Determination Kit (Sigma) and Cholesterol Assay Kit (Cayman), respectively. The assay plates were read by a TECAN M200 instrument (Tecan) following the manufacturer's instructions.

Glucose tolerance and insulin tolerance tests (GTT and ITT). Glucose tolerance test (GTT) and insulin tolerance test (ITT) were performed largely as described (He et al., 2015; Jeong et al., 2015). Briefly, after overnight and 5-hr fasting, GTT and ITT were conducted at ZT2 and ZT8 respectively. Glucose levels were measured from tail blood before and 15, 30, 60, or 120 min after injection of either 1 g/kg glucose or 0.75 U/kg insulin (Sigma) at ZT2 and ZT8 respectively by using the ONETOUCH UltraMini blood glucose monitoring system (LifeScan). Serum insulin levels were measured with the Rat/Mouse Insulin Elisa kit (Millipore) according to the

manufacturer's instructions. The plasma samples were collected at ZT2 as described above for lipid assays.

Histological analysis of liver and adipose tissues. For microscopic analysis of lipid accumulation in liver, tissue samples were collected and immediately embedded in Tissue-Tek OCT cryostat molds (Leica) and then frozen at -80°C. Tissue sections were stained in 0.5% Oil Red O and counterstained with Mayer's hematoxylin for 1 min. In addition, liver, brown fat and white fat tissues were embedded in paraffin and stained with Hematoxylin and Eosin (H&E). Microscopic images were obtained on an Olympus BX60 microscope.

Real-time qPCR and Western blot analyses. For qPCR analysis, cells were split into 6-well plates at an initial density of 3X 10^5 cells and incubated for 2-4 days before synchronization (5μM Fsk or 100nM Dex) followed by compound treatment. RNA samples were prepared by using PureXtract RNAsol for cDNA synthesis and real-time PCR (GenDEPOT) was performed with a MaxPro3000 Thermocycler (Agilent). qPCR primers used are listed in Table S1. Whole-cell lysates from cells similarly grown and treated in 60mm dishes and tissue extracts were prepared as described (Yoo et al., 2013) and subjected to Western blot analysis (GenDEPOT). Antibodies for REV-ERBα (Pierce and Cell Signaling), PER1 (Lee et al., 2001) and other clock proteins (Yoo et al., 2013) were used.

Microarray analysis. Total RNAs prepared from liver tissues from RC-fed, Vehicle-treated and HFD-fed, Vehicle or NOB-treated WT mice for 10 weeks were reverse transcribed into cDNAs, which were then biotin-UTP labeled and hybridized to the Illumina mouse WG-6v2.0 Expression BeadChip. Genes with statistically significant fold change differences was clustered using centered correlation (Cluster 3.0) and then visualized as a heat map on Tree View. Moreover, genes with statistically significant differences derived from microarray analyses were imported into the Ingenuity Pathway Analysis (IPA, http://www.ingenuity.com). In IPA, differentially expressed genes are mapped to genetic networks in the Ingenuity Knowledge Database to generate a set of network and then ranked by score. Heatmaps were generated by using Cluster 3.0 program. ChIP-seq data analysis was conducted as previously described (Koike et al., 2012). The data discussed in this publication have been deposited in NCBI's Gene Expression Omnibus (Edgar et al., 2002) and are accessible through GEO Series accession number GSE78848 (https://www.ncbi.nlm.nih.gov/geo/query/acc.cgi?acc=GSE78848).

Plasmids. Plasmids containing the retinoic acid-related orphan receptor response element (RORE) from mouse *Bmal1* promoter, pcDNA3.1B-G4DBD-RORαLBD and pcDNA3.1B-G4DBD-RORγLBD were constructed in our lab. Specifically, the 1960bp sequences (-1830/+130) of the mouse *Bmal1* promoter harboring either WT (AAAGTAGGTCA and AAAGTAGGTTA) or mutant (AAAGTACACGA) RORE were PCR amplified from mouse genomic DNA and cloned into pGL3-promoter luciferase vector. For expression of RORα or RORγ-GAL4 protein, mouse RORα-LBD (aa 261-523) or RORγ-LBD (aa 250-516) were PCR amplified from mouse genomic DNA and cloned into a GAL4-DBD-containing vector, pcDNA3.1B.

One-hybrid reporter assays. For mammalian one-hybrid assays, HEK293T cells were co-transfected with pcDNA3.1B-G4DBD-RORα/γLBD, pGL4.31 and TK promoter Renilla luciferase construct (tK.pRL). To investigate the regulation of the Bmal1 reporter, Hepa1-6 cells were co-transfected with Bmal1-WT or mutant RORE reporter plasmids, RORα, RORγ or Rev-erbα expression construct along with tK.pRL. Mouse and human siRNA targeting RORα and RORγ were purchased from Santa Cruz. Transfection was performed by Lipfectamine 2000 reagent (Invitrogen) Twenty-four hours after transfection, the cells were treated with vehicle or NOB.

Lysates were collected 24h after treatment, and firefly and *Renilla* luciferase activities were measured by using a Dual-Luciferase Reporter System (Promega). Regardless of the nature of the ligand (agonist or inverse agonist), ligand interaction with these chimeric receptors has been shown to reduce transcriptional activity of these chimeric receptors (Wang et al., 2010a; Wang et al., 2010b).

Radioligand receptor binding assays. We adopted previously described protocols with minor modifications (Kumar et al., 2010; Wang et al., 2010b). For saturation binding experiments, 100ng RORα-LBD or 200ng RORγ-LBD was incubated with 25-[^{3}H]-hydroxycholesterol (OHC) in assay buffer [50mM HEPES, pH. 7.4, 0.05% bovine serum albumin (BSA), 150mM NaCl and 5mM MgCl2]. Ligand binding was determined by filter binding assays to calculate the Kd value. For competitive binding assay, 100ng RORα-LBD or 200ng RORγ-LBD was incubated with various concentrations of Nobiletin, Naringin or Naringenin in the presence of 4.5 nM 25-[^{3}H]-OHC. K_i was determined using the Cheng-Prusoff equation.

RNA-mediated interference. Hepa1-6 cells on the 24-well plate were transfected using control siRNA and siRNA against mouse RORα and RORγ (Santa Cruz). Twenty four hours after transfection, cells were treated with DMSO or NOB (3 μM). After 12hr treatment, cells were harvested and total RNA was insolated. Real-time qPCR was performed to analyze the mRNA expression of mouse *Rora* and *Rorc* with a MaxPro3000 Thermocycler (Agilent).

Statistical analysis. Data are presented as mean ± SEM. Statistical significance was determined by one-way or two-way ANOVA with Turkey's and Dunnett's tests for multiple group comparisons. $P<0.05$ was considered to be statistically significant.

Legends for Supplemental Data files

Data S1, related to Figure 5. List of up-regulated (fold change $\geqslant$2.00) and down-regulated (fold change $\leqslant$0.50) genes identified in the microarray analysis. Four comparison groups are listed, including HF.Veh vs. RC and HF.NOB vs. HF.Veh at both ZT2 and ZT14. Fold change of 1.00 indicates no difference in expression levels.

Data S2, related to Figure 5. Function classification of NOB-responsive genes showing reversal of HFD-induced expression changes by NOB at ZT2 and/or ZT14. This gene set was annotated from a total of 251 genes.

Supplemental References

Antoch, M.P., Song, E.J., Chang, A.M., Vitaterna, M.H., Zhao, Y., Wilsbacher, L.D., Sangoram, A.M., King, D.P., Pinto, L.H., and Takahashi, J.S. (1997). Functional identification of the mouse circadian Clock gene by transgenic BAC rescue. Cell *89*, 655-667.

Chen, Z., Yoo, S.H., Park, Y.S., Kim, K.H., Wei, S., Buhr, E., Ye, Z.Y., Pan, H.L., and Takahashi, J.S. (2012). Identification of diverse modulators of central and peripheral circadian clocks by high-throughput chemical screening. Proc Natl Acad Sci U S A *109*, 101-106.

Chutkow, W.A., Birkenfeld, A.L., Brown, J.D., Lee, H.Y., Frederick, D.W., Yoshioka, J., Patwari, P., Kursawe, R., Cushman, S.W., Plutzky, J.*, et al.* (2010). Deletion of the alpha-arrestin protein Txnip in mice promotes adiposity and adipogenesis while preserving insulin sensitivity. Diabetes *59*, 1424-1434.
Daniels, I.S., Zhang, J., O'Brien, W.G., 3rd, Tao, Z., Miki, T., Zhao, Z., Blackburn, M.R., and Lee, C.C. (2010). A role of erythrocytes in adenosine monophosphate initiation of hypometabolism in mammals. The Journal of biological chemistry *285*, 20716-20723.
Edgar, R., Domrachev, M., and Lash, A.E. (2002). Gene Expression Omnibus: NCBI gene expression and hybridization array data repository. Nucleic Acids Res *30*, 207-210.
Garcia, J.M., Scherer, T., Chen, J.A., Guillory, B., Nassif, A., Papusha, V., Smiechowska, J., Asnicar, M., Buettner, C., and Smith, R.G. (2013). Inhibition of cisplatin-induced lipid catabolism and weight loss by ghrelin in male mice. Endocrinology *154*, 3118-3129.
He, B., Nohara, K., Ajami, N.J., Michalek, R.D., Tian, X., Wong, M., Losee-Olson, S.H., Petrosino, J.F., Yoo, S.H., Shimomura, K.*, et al.* (2015). Transmissible microbial and metabolomic remodeling by soluble dietary fiber improves metabolic homeostasis. Sci Rep *5*, 10604.
Jeong, K., He, B., Nohara, K., Park, N., Shin, Y., Kim, S., Shimomura, K., Koike, N., Yoo, S.H., and Chen, Z. (2015). Dual attenuation of proteasomal and autophagic BMAL1 degradation in Clock(Delta19/+) mice contributes to improved glucose homeostasis. Sci Rep *5*, 12801.
King, D.P., Zhao, Y., Sangoram, A.M., Wilsbacher, L.D., Tanaka, M., Antoch, M.P., Steeves, T.D., Vitaterna, M.H., Kornhauser, J.M., Lowrey, P.L.*, et al.* (1997). Positional cloning of the mouse circadian clock gene. Cell *89*, 641-653.
Koike, N., Yoo, S.H., Huang, H.C., Kumar, V., Lee, C., Kim, T.K., and Takahashi, J.S. (2012). Transcriptional architecture and chromatin landscape of the core circadian clock in mammals. Science *338*, 349-354.
Kumar, A., Devaraj, V.C., Giri, K.C., Giri, S., Rajagopal, S., and Mullangi, R. (2012). Development and validation of a highly sensitive LC-MS/MS-ESI method for the determination of nobiletin in rat plasma: application to a pharmacokinetic study. Biomed Chromatogr *26*, 1464-1471.
Kumar, N., Solt, L.A., Conkright, J.J., Wang, Y., Istrate, M.A., Busby, S.A., Garcia-Ordonez, R.D., Burris, T.P., and Griffin, P.R. (2010). The benzenesulfoamide T0901317 [N-(2,2,2-trifluoroethyl)-N-[4-[2,2,2-trifluoro-1-hydroxy-1-(trifluoromethyl)ethy l]phenyl]-benzenesulfonamide] is a novel retinoic acid receptor-related orphan receptor-alpha/gamma inverse agonist. Mol Pharmacol *77*, 228-236.
Lee, C., Etchegaray, J.P., Cagampang, F.R., Loudon, A.S., and Reppert, S.M. (2001). Posttranslational mechanisms regulate the mammalian circadian clock. Cell *107*, 855-867.
Lee, Y.S., Cha, B.Y., Choi, S.S., Choi, B.K., Yonezawa, T., Teruya, T., Nagai, K., and Woo, J.T. (2013). Nobiletin improves obesity and insulin resistance in high-fat diet-induced obese mice. J Nutr Biochem *24*, 156-162.
Li, R.W., Theriault, A.G., Au, K., Douglas, T.D., Casaschi, A., Kurowska, E.M., and Mukherjee, R. (2006). Citrus polymethoxylated flavones improve lipid and glucose homeostasis and modulate adipocytokines in fructose-induced insulin resistant hamsters. Life Sci *79*, 365-373.
Liu, Y., Zhou, D., Zhang, F., Tu, Y., Xia, Y., Wang, H., Zhou, B., Zhang, Y., Wu, J., Gao, X.*, et al.* (2012). Liver Patt1 deficiency protects male mice from age-associated but not high-fat diet-induced hepatic steatosis. Journal of lipid research *53*, 358-367.
Schmid, B., Helfrich-Forster, C., and Yoshii, T. (2011). A new ImageJ plug-in "ActogramJ" for chronobiological analyses. J Biol Rhythms *26*, 464-467.
Singh, S.P., Wahajuddin, Tewari, D., Patel, K., and Jain, G.K. (2011). Permeability determination and pharmacokinetic study of nobiletin in rat plasma and brain by validated high-performance liquid chromatography method. Fitoterapia *82*, 1206-1214.

Wang, Y., Kumar, N., Nuhant, P., Cameron, M.D., Istrate, M.A., Roush, W.R., Griffin, P.R., and Burris, T.P. (2010a). Identification of SR1078, a synthetic agonist for the orphan nuclear receptors RORalpha and RORgamma. ACS Chem Biol *5*, 1029-1034.
Wang, Y., Kumar, N., Solt, L.A., Richardson, T.I., Helvering, L.M., Crumbley, C., Garcia-Ordonez, R.D., Stayrook, K.R., Zhang, X., Novick, S*., et al.* (2010b). Modulation of retinoic acid receptor-related orphan receptor alpha and gamma activity by 7-oxygenated sterol ligands. The Journal of biological chemistry *285*, 5013-5025.
Yoo, S.H., Mohawk, J.A., Siepka, S.M., Shan, Y., Huh, S.K., Hong, H.K., Kornblum, I., Kumar, V., Koike, N., Xu, M*., et al.* (2013). Competing E3 ubiquitin ligases govern circadian periodicity by degradation of CRY in nucleus and cytoplasm. Cell *152*, 1091-1105.
Zheng, B., Larkin, D.W., Albrecht, U., Sun, Z.S., Sage, M., Eichele, G., Lee, C.C., and Bradley, A. (1999). The mPer2 gene encodes a functional component of the mammalian circadian clock. Nature *400*, 169-173.